Collectivity of the 2_1^+ state in $Z \leqslant 82$ even-even nuclei probed by a ratio involving dynamic and static electromagnetic $E2$ moments: Evolution of the quadrupole degrees of freedom and a new signature for shape coexistence

P. Petkov [1], D.-S. Delion [1], and C. Müller-Gatermann [2,*]

[1] *"Horia Hulubei" National Institute Nuclear Engineering R-76900 Bucharest-Măgurele, Romania*

[2] *Insitut für Kernphysik der Universität zu Köln, D-50937 Cologne, Germany*

(Received 24 June 2020; revised 9 September 2020; accepted 25 September 2020; published 14 October 2020)

We present a new approach to investigate the evolution of collectivity on the nuclear map based on the ratio $R = B(E2; 2_1^+ \to 0_1^+)_{\rm exp}/B(E2; 2_1^+ \to 0_1^+)_Q$, where the quantity in the denominator is calculated using the quadrupole moment of the 2_1^+ level when known. The systematics of such ratios in even-even nuclei reveals interesting features including signatures for particular collective excitations and sensitivity to shell- and subshell closures. A reproduction of these data by theoretical models is highly desirable with the potential to shed more light on the interplay between collective and single-particle motions. In particular, a new signature for shape coexistence was found: $R < 1$.

DOI: 10.1103/PhysRevC.102.044317

I. INTRODUCTION

Nuclei are examples of quantum systems with a relatively small number of constituent particles appealing for finding solutions of the many-body quantum problem [1] on the basis of the knowledge of the fundamental interactions. Nowadays, *ab initio* calculations are feasible until mass number $A \approx 40$. Developments within the shell model (see, e.g., [2]), with some separation of valence and core nucleons, allow to significantly extend its application range [3]. The latter separation is similar to that in the generalized collective model [4] where, however, the core may undergo collective excitations of vibrational and rotational type. Therefore the notion of nuclear shape in a geometrical sense naturally emerges within that model. Insight into such shapes can be gained also on the basis of, e.g., shell-model calculations by determining in three dimensions the geometrical characteristics of the space region where the nucleons are confined or by considering collective potentials associated with vibrations/rotations. Thus, in medium and heavy nuclei, taking into account the effects of collective and single-particle degrees of freedom as well as their interplay is the most common approach to study nuclear structure. The lowest order deviations from spherical shape are quadrupole deformations which are described in the body-fixed coordinate system in terms of the dynamic variables/parameters β (associated with the degree of the overall deformation) and γ (describing the motion or rigid shape away from axial symmetry) [4]. In the present work, we address the simplest quadrupole excitations by considering the systematics of electromagnetic observables characterizing the first excited 2^+ states in even-even nuclei and more precisely, that of a new experimental quantity, a ratio, derived using these observables. Systematics of similar kind were already discussed in the literature [5,6] but we believe that the our work presents some new features which may be used for a more sensitive classification/assignment of excitation modes.

II. FORMALISM AND DEFINITION OF THE NEW RATIO

We start with some identities related to the basic electromagnetic observables, namely the reduced $B(E2)$ transition strength to the ground state and the quadrupole moment $Q(2_1^+)$, which are used later. In axially symmetric nuclei the rotational model predicts

$$B(E2; 2_1^+ \to 0_1^+) = \frac{|<0_1^+||E2||2_1^+>|^2}{5} = \frac{5}{16\pi} <2020|00>^2 Q_0^2, \quad (1)$$

where Q_0 is the intrinsic quadrupole moment in the body-fixed coordinate system. For shapes differing from axial symmetry and somewhat phenomenologically, a new quantity, the transition quadrupole moment Q_t is often introduced which simply replaces Q_0 in Eq. (1), especially at higher spins. Another quadrupole observable is the spectroscopic quadrupole moment Q which can also be experimentally determined. In a spherical coordinate system the z component of the quadrupole operator is expressed as

$$\tilde{Q}_z = \sqrt{\frac{16\pi}{5}} \Sigma_{i=1}^A e_i r_i^2 Y_2^0(\theta_i, \phi_i), \quad (2)$$

where the sum runs over the nucleons. Its reduced matrix element between the 2_1^+ and 0_1^+ states is related to Q_0 via

$$\langle 0_1^+||\tilde{Q}_z||2_1^+\rangle = \sqrt{\frac{25}{16\pi}} \langle 2020|00\rangle Q_0. \quad (3)$$

*Present address: Argonne National Laboratory, 9700 S. Cass Avenue Lemont, Il 60439, USA.

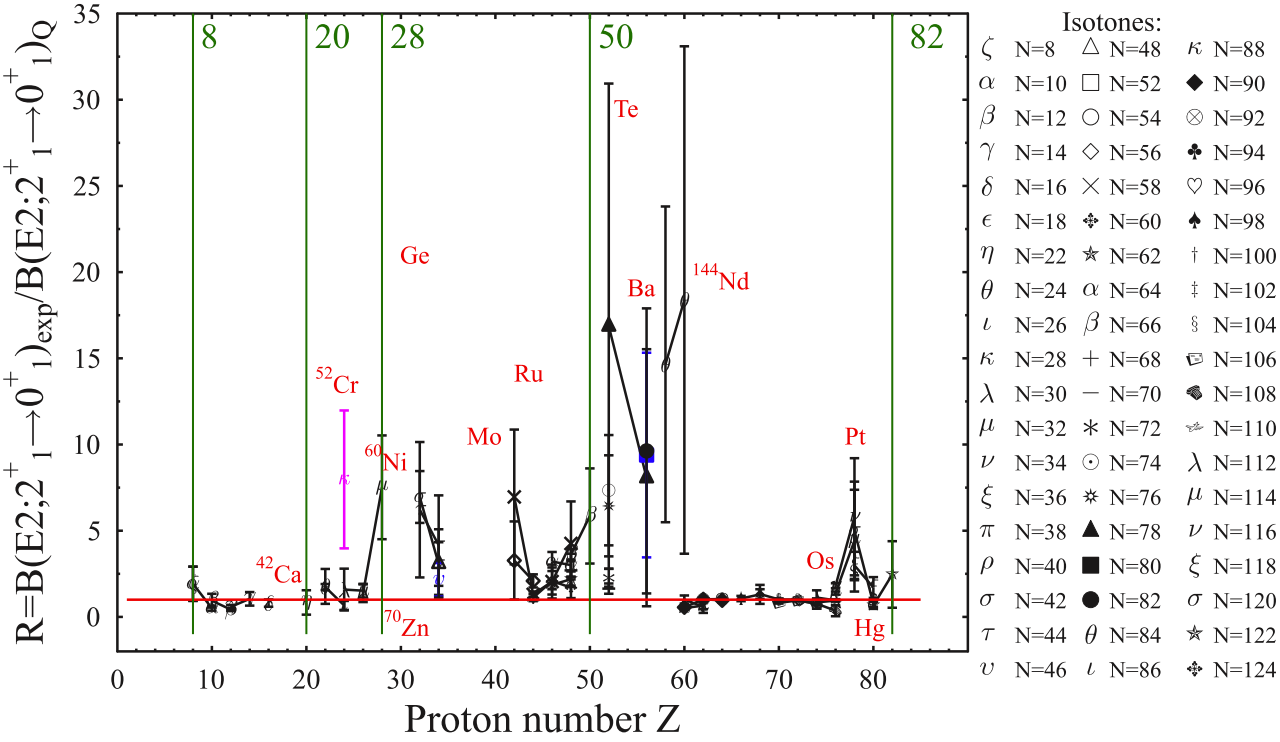

FIG. 1. Ratio R for even-even nuclei from $Z = 6$ to $Z = 82$ with known quadrupole moments of the 2^+_1 levels. The data on $B(E2)$'s and Q's are taken from Ref. [5] where experimental results published in recent surveys are summarized. The only exceptions are these of ^{20,22}Ne [7] and ^{30,32}S [8]. The line corresponding to an axially symmetric rotor (ASR) with $R = 1$ is also shown. The legend indicates the isotones interconnected by lines in the figure. See also text.

The spectroscopic quadrupole moment of a nuclear state with spin I is proportional to the reduced static matrix element of the spherical tensor of second rank $\tilde{Q}$ (i.e., of the operator for $E2$ transitions)

$$Q(I) = \langle I, m = I|\tilde{Q}_z|I, m = I\rangle = \sqrt{\frac{I(2I-1)}{(2I+1)(2I+3)(I+1)}}\langle I||\tilde{Q}_z||I\rangle. \quad (4)$$

In the case of rotation of an axially deformed nucleus this expression reduces to

$$Q = \frac{3K^2 - I(I+1)}{(I+1)(2I+3)}Q_0, \quad (5)$$

where K is the projection of the angular momentum on the symmetry axis. Thus, for the first excited 2^+ state, the first member of the $K = 0$ rotational band built on the ground state, one obtains

$$Q(2^+_1) = -\tfrac{2}{7}Q_0(2^+_1). \quad (6)$$

Therefore it is easy to employ the spectroscopic quadrupole moment Q to "extract" Q_0 and calculate a value of a $B(E2)$ transition strength via Eqs. (6),(1), namely, the expression reads

$$B(E2; 2^+_1 \to 0^+_1)_Q = \frac{5}{16\pi}\left(\frac{7}{2}\right)^2\langle 2020|00\rangle^2 Q^2. \quad (7)$$

This new quantity $B(E2)_Q$, although not a real observable, can be considered as "experimental" since it is proportional to the square of the measured quadrupole moment Q. Thus, one can define a ratio R of the experimental $B(E2)_{\rm exp}$ value to the value $B(E2)_Q$ calculated using Q:

$$R = \frac{B(E2)_{\rm exp}}{B(E2)_Q}. \quad (8)$$

Deviations of this value from $R = 1$ (ASR horizontal line in Figs. 1, 2 and below) point to other shapes or collective and single-particle degrees of freedom in the particular nucleus compared to the simple rotation of the nucleon "fluid" composed by some part of the constituents of the nucleus.

III. DISCUSSION OF THE SYSTEMATICS

In Fig. 1, we present the ratio R for nuclei with known $Q(2^+_1)$ in the region $Z \leqslant 82$ in dependence from the number of protons Z, and in Fig. 2 the same data as function of the number of neutrons N. The data on Q's and $B(E2)$'s were taken from the recent systematics [5]. However, we decided to employ in our considerations only data with relative uncertainty $\frac{\Delta R}{R} \leqslant 100\%$. This excludes some of the data points [5], mainly due to quadrupole moments (negative or positive) with small modulus which are the most difficult to determine experimentally. In Figs. 3,4, and5, we present the Nilsson schemes relevant for the number of nucleons involving in the present study.

Our considerations are very close the ideas developed earlier by Robinson *et al.* in [6], where, however, the ratio of the intrinsic quadrupole moment derived from the measured

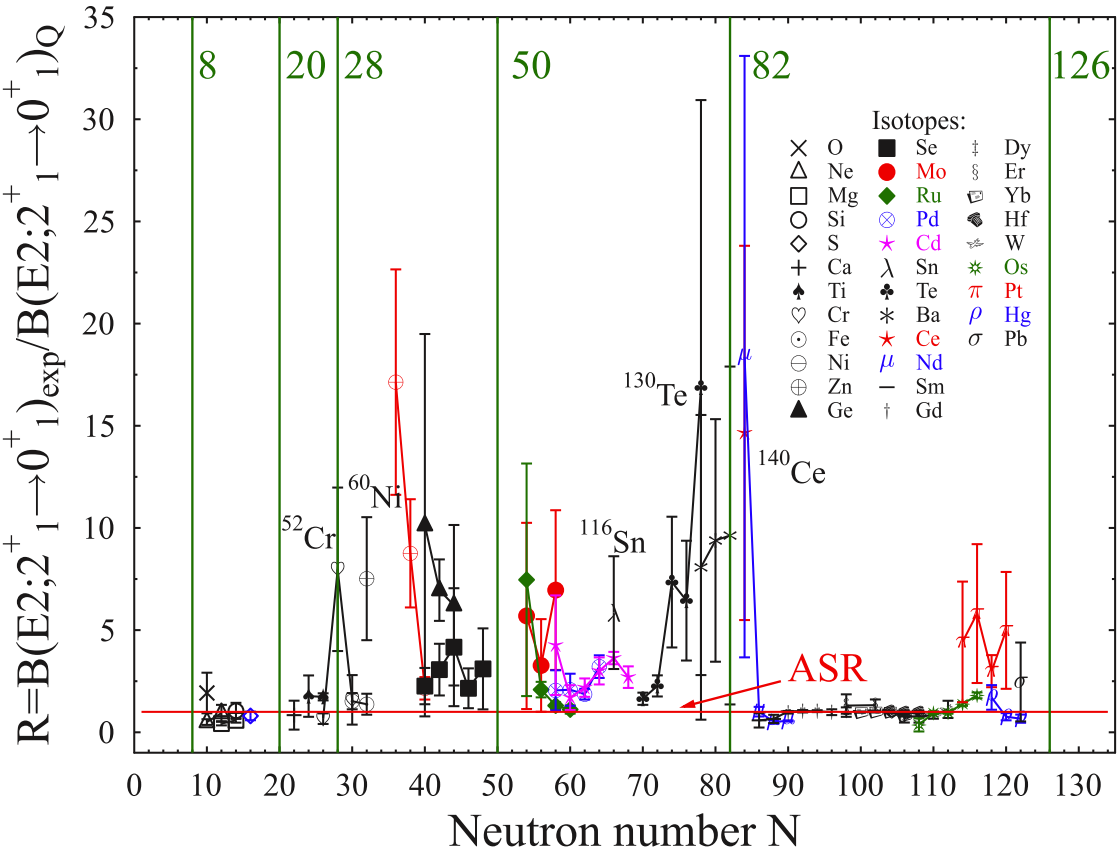

FIG. 2. The same data as in Fig. 1 but displayed as a function of the number of neutrons N. The isotopes of the different elements are interconnected by lines. See also text.

spectroscopic quadrupole moment via Eq. (6) and the intrinsic quadrupole moment derived using Eq. (1) from the experimental $B(E2)$ data is considered. We shall denote this ratio by

$$R_{Q_0Q_0} = \sqrt{\frac{49}{64\pi}} Q(2_1^+) \Big/ \sqrt{B(E2; 2_1^+ \to 0_1^+)}. \qquad (9)$$

It should be mentioned, as the authors of [6] do, that the equations used to derive Eq. (9) are valid for axially symmetric rotors and thus are not necessarily valid for every possible nuclear shape. Therefore also the $B(E2)_Q$ value calculated by us using Eq. (1) represents simply an auxiliary/helping quantity used for normalization/comparison such as the considerations below. It should be mentioned that the work [6] was dedicated not to a systematic study of $R_{Q_0Q_0}$ across the nuclear map but rather to a group of light nuclei close to and in the fp shell, within the the context of shell-model tests of rotational-model relations. The very recent systematics published by Sharon *et al.* [5] employed the ratio

$$R_{QB} = \frac{Q(2_1^+)}{\sqrt{B(E2; 0_1^+ \to 2_1^+)}} \qquad (10)$$

which was investigated in the same range of nuclei as in our study. Within the rotational model already discussed $R_{QB} = -0.906$, i.e., a quantity whose modulus is close to 1 [5]. One advantage of this approach is that only purely experimental quantities are used to define the ratio. But when the nuclei considered deviate from this limit, the simplicity of the relation between $Q(2+)$ and the square root of the $B(E2)$ gets lost. This is because there is not a universal relation between the diagonal reduced $E2$ matrix element related precisely to $Q(2+)$ and the off-diagonal reduced $E2$ matrix element connecting the $2+$ and $0+$ states. The ratio R_{QB} cannot be mathematically related to our ratio R in a simple way apart the axial rigid rotor limit. But even in this case the transformation is not linear, it is quadratic. Another advantage of Eq. (10) is the sign of the ratio which may be both negative and positive keeping the information on closeness of Q to the prolate or oblate limits, respectively. As commented in Ref. [5], the R_{QB} values form mainly two distinct groups: one with values scattered around to the rotational limit of -0.906 and another one, characterized by a much bigger variance, scattered roughly around the value $R_{QB} = -0.5$. By an optical investigation of the mass number and elemental dependence of R_{QB} shown in Fig. 1 of Ref. [5] one can easily associate the latter group with vibrational and more or less transitional nuclei with few exceptions. The ratio R used in the present work emphasizes the cases of large excursions from the rotational model in cases of measured quadrupole moments with small modulus as well as the cases $R < 1$ (see below).

The results of the calculations of R are summarized in Table I. Below we will consider them, first concentrating on the effects whose single particle nature is easy to gain close

TABLE I. In the first three columns, the nuclide is identified by Z, N, and A, respectively. The experimental data with their uncertainties on the spectroscopic quadrupole moments Q (given in eb) and the $B(E2; 2_1^+ \to 0_1^+)$ transition strengths (in e^2b^2) are displayed in the next four columns. The ratio R and and its error ΔR are shown in columns 7 and 8, respectively. In the next columns are displayed N_π, N_ν, their product N_π, N_ν, and the distances from the closest magic numbers for the number of protons Z and neutrons N in terms of IBA [9] bosons, and the distances from the closest magic numbers for the number of protons Z and neutrons N in terms of IBA [9] bosons, and finally, the normalized product $P = \frac{N_\pi N_\nu}{N_\pi + N_\nu}$ (the so-called P factor [22]). See also text.

Z	N	A	Q	ΔQ	$B(E2)$	$dB(E2)$	R	ΔR	N_π	N_ν	$N_\pi N_\nu$	Z-$Z_{\text{magic}-1}$	Z_{magic}-Z	N-$N_{\text{magic}-1}$	N_{magic}-N	$\frac{N_\pi N_\nu}{N_\pi + N_\nu}$
8	8	16	−0.040	0.010	0.001	0.000	2.21	1.12	0	0	0	0	6	0	6	0.00
10	10	20	−0.230	0.030	0.006	0.001	0.50	0.14	1	1	1	1	5	1	5	0.50
10	12	22	−0.190	0.040	0.008	0.001	0.94	0.40	1	2	2	1	5	2	4	0.67
12	12	24	−0.290	0.030	0.009	0.000	0.43	0.09	2	2	4	2	4	2	4	1.00
12	14	26	−0.210	0.020	0.006	0.000	0.58	0.11	2	3	6	2	4	3	3	1.20
14	14	28	0.160	0.030	0.019	0.000	2.97	1.11	3	3	9	3	3	3	3	1.50
16	16	32	−0.160	0.020	0.005	0.000	0.80	0.21	2	2	4	4	2	4	2	1.00
20	22	42	−0.190	0.080	0.019	0.001	2.16	1.82	0	1	0	0	4	1	3	0.00
22	24	46	−0.210	0.060	0.019	0.001	1.77	1.01	1	2	2	1	3	2	2	0.67
22	26	48	−0.180	0.010	0.013	0.001	1.68	0.20	1	1	1	1	3	3	1	0.50
24	26	50	−0.360	0.070	0.021	0.001	0.67	0.26	2	1	2	2	2	3	1	0.67
24	28	52	−0.080	0.020	0.012	0.001	7.98	4.00	2	0	0	2	2	0	11	0.00
24	30	54	−0.210	0.080	0.017	0.001	1.59	1.21	2	1	2	2	2	1	10	0.67
26	30	56	−0.230	0.030	0.020	0.000	1.52	0.40	1	1	1	3	1	1	10	0.50
26	32	58	−0.270	0.050	0.024	0.001	1.37	0.51	1	2	2	3	1	2	9	0.67
28	32	60	−0.100	0.020	0.018	0.000	7.52	3.01	0	2	0	0	11	2	9	0.00
30	40	70	−0.240	0.030	0.030	0.002	2.15	0.55	1	5	5	1	10	6	5	0.83
32	40	72	−0.130	0.060	0.042	0.001	10.13	9.36	2	5	10	2	9	6	5	1.43
32	42	74	−0.190	0.020	0.061	0.003	6.96	1.50	2	4	8	2	9	7	4	1.33
32	44	76	−0.190	0.060	0.055	0.001	6.22	3.93	2	3	6	2	9	8	3	1.20
34	40	74	−0.360	0.070	0.071	0.004	2.26	0.89	3	5	15	3	8	6	5	1.88
34	42	76	−0.340	0.070	0.086	0.003	3.07	1.27	3	4	12	3	8	7	4	1.71
34	44	78	−0.260	0.090	0.069	0.002	4.16	2.89	3	3	9	3	8	8	3	1.50
34	46	80	−0.310	0.070	0.050	0.002	2.15	0.97	3	2	6	3	8	9	2	1.20
34	48	82	−0.220	0.070	0.037	0.002	3.10	1.98	3	1	3	3	8	10	1	0.75
42	54	96	−0.200	0.080	0.056	0.001	5.69	4.56	4	2	8	7	4	2	14	1.33
42	56	98	−0.260	0.090	0.054	0.001	3.27	2.27	4	3	12	7	4	3	13	1.71
42	58	100	−0.250	0.070	0.106	0.005	6.96	3.91	4	4	16	7	4	4	12	2.00
44	54	98	−0.210	0.080	0.080	0.003	7.46	5.69	3	2	6	8	3	2	14	1.20
44	56	100	−0.440	0.040	0.099	0.001	2.09	0.38	3	3	9	8	3	3	13	1.50
44	58	102	−0.630	0.040	0.126	0.002	1.31	0.17	3	4	12	8	3	4	12	1.71
44	60	104	−0.780	0.070	0.165	0.003	1.11	0.20	3	5	15	8	3	5	11	1.88
46	58	104	−0.460	0.110	0.106	0.003	2.05	0.98	2	4	8	9	2	4	12	1.33
46	60	106	−0.510	0.070	0.132	0.034	2.08	0.78	2	5	10	9	2	5	11	1.43
46	62	108	−0.580	0.040	0.153	0.004	1.86	0.26	2	6	12	9	2	6	10	1.50
46	64	110	−0.470	0.040	0.173	0.005	3.21	0.55	2	7	14	9	2	7	9	1.56
48	58	106	−0.280	0.080	0.081	0.002	4.26	2.44	1	4	4	10	1	4	12	0.80
48	60	108	−0.450	0.080	0.084	0.003	1.70	0.61	1	5	5	10	1	5	11	0.83
48	62	110	−0.400	0.040	0.085	0.004	2.19	0.45	1	6	6	10	1	6	10	0.86
48	64	112	−0.370	0.040	0.100	0.004	3.00	0.66	1	7	7	10	1	7	9	0.88
48	66	114	−0.350	0.010	0.107	0.005	3.59	0.26	1	8	8	10	1	8	8	0.89
48	68	116	−0.420	0.040	0.116	0.005	2.70	0.53	1	7	7	10	1	9	7	0.88
50	66	116	−0.170	0.040	0.041	0.001	5.86	2.76	0	8	0	0	16	8	8	0.00
52	70	122	−0.570	0.050	0.130	0.006	1.64	0.30	1	6	6	1	15	10	6	0.86
52	72	124	−0.450	0.050	0.112	0.006	2.27	0.52	1	5	5	1	15	11	5	0.83
52	74	126	−0.230	0.050	0.095	0.002	7.35	3.20	1	4	4	1	15	12	4	0.80
52	76	128	−0.220	0.050	0.076	0.001	6.44	2.93	1	3	3	1	15	13	3	0.75
52	78	130	−0.120	0.050	0.059	0.002	16.87	14.07	1	2	2	1	15	14	2	0.67
56	78	134	−0.260	0.120	0.133	0.004	8.07	7.46	3	2	6	3	13	14	2	1.20
56	80	136	−0.190	0.060	0.083	0.002	9.39	5.93	3	1	3	3	13	15	1	0.75
56	82	138	−0.140	0.060	0.046	0.002	9.63	8.27	3	0	0	3	13	0	22	0.00
58	84	142	−0.160	0.050	0.091	0.001	14.65	9.16	4	1	4	4	12	1	21	0.80

TABLE I. (*Continued.*)

Z	N	A	Q	ΔQ	$B(E2)$	$dB(E2)$	R	ΔR	N_π	N_ν	$N_\pi N_\nu$	Z-$Z_{\text{magic}-1}$	Z_{magic}-Z	N-$N_{\text{magic}-1}$	N_{magic}-N	$\frac{N_\pi N_\nu}{N_\pi+N_\nu}$
60	84	144	−0.150	0.060	0.101	0.003	18.38	14.72	5	1	5	5	11	1	21	0.83
60	86	146	−0.780	0.090	0.150	0.004	1.01	0.23	5	2	10	5	11	2	20	1.43
60	88	148	−1.460	0.130	0.268	0.006	0.52	0.09	5	3	15	5	11	3	19	1.88
60	90	150	−2.000	0.050	0.541	0.006	0.56	0.03	5	4	20	5	11	4	18	2.22
62	86	148	−1.000	0.300	0.143	0.007	0.59	0.35	6	2	12	6	10	2	20	1.50
62	88	150	−1.300	0.200	0.269	0.005	0.65	0.20	6	3	18	6	10	3	19	2.00
62	90	152	−1.670	0.020	0.692	0.000	1.02	0.02	6	4	24	6	10	4	18	2.40
62	92	154	−1.870	0.040	0.869	0.001	1.02	0.04	6	5	30	6	10	5	17	2.73
64	90	154	−1.820	0.040	0.774	0.000	0.96	0.04	7	4	28	7	9	4	18	2.55
64	92	156	−1.930	0.040	0.940	0.022	1.04	0.05	7	5	35	7	9	5	17	2.92
64	94	158	−2.010	0.040	1.018	0.022	1.03	0.05	7	6	42	7	9	6	16	3.23
64	96	160	−2.080	0.150	1.037	0.003	0.98	0.14	7	7	49	7	9	7	15	3.50
66	98	164	−2.080	0.150	1.123	0.014	1.07	0.15	8	8	64	8	8	8	14	4.00
68	98	166	−1.900	0.400	1.145	0.009	1.30	0.55	7	8	56	9	7	8	14	3.73
68	102	170	−1.900	0.200	1.168	0.016	1.33	0.28	7	10	70	9	7	10	12	4.12
70	100	170	−2.180	0.030	1.145	0.009	0.99	0.03	6	9	54	10	6	9	13	3.60
70	102	172	−2.220	0.040	1.218	0.030	1.01	0.04	6	10	60	10	6	10	12	3.75
70	104	174	−2.180	0.050	1.170	0.032	1.01	0.05	6	11	66	10	6	11	11	3.88
70	106	176	−2.280	0.060	1.038	0.018	0.82	0.05	6	10	60	10	6	12	10	3.75
72	104	176	−2.100	0.020	1.084	0.034	1.01	0.04	5	11	55	11	5	11	11	3.44
72	106	178	−2.020	0.020	0.947	0.013	0.95	0.02	5	10	50	11	5	12	10	3.33
72	108	180	−2.000	0.020	0.929	0.001	0.95	0.02	5	9	45	11	5	13	9	3.21
74	106	180	−2.100	0.400	0.830	0.028	0.77	0.30	4	10	40	12	4	12	10	2.86
74	108	182	−2.100	0.400	0.825	0.008	0.77	0.29	4	9	36	12	4	13	9	2.77
74	110	184	−1.900	0.200	0.741	0.007	0.84	0.18	4	8	32	12	4	14	8	2.67
74	112	186	−1.600	0.300	0.700	0.008	1.12	0.42	4	7	28	12	4	15	7	2.55
76	108	184	−2.700	1.200	0.643	0.016	0.36	0.32	3	9	27	13	3	13	9	2.25
76	110	186	−1.630	0.040	0.613	0.014	0.95	0.05	3	8	24	13	3	14	8	2.18
76	112	188	−1.460	0.040	0.500	0.007	0.96	0.05	3	7	21	13	3	15	7	2.10
76	114	190	−1.180	0.030	0.469	0.018	1.38	0.09	3	6	18	13	3	16	6	2.00
76	116	192	−0.960	0.030	0.406	0.020	1.81	0.14	3	5	15	13	3	17	5	1.88
78	114	192	0.600	0.200	0.388	0.013	4.42	2.95	2	6	12	14	2	16	6	1.50
78	116	194	0.480	0.140	0.326	0.014	5.81	3.40	2	5	10	14	2	17	5	1.43
78	118	196	0.620	0.080	0.280	0.014	2.99	0.79	2	4	8	14	2	18	4	1.33
78	120	198	0.420	0.120	0.214	0.010	4.99	2.86	2	3	6	14	2	19	3	1.20
80	118	198	0.680	0.120	0.192	0.001	1.71	0.60	1	4	4	15	1	18	4	0.80
80	120	200	0.960	0.110	0.171	0.006	0.76	0.18	1	3	3	15	1	19	3	0.75
80	122	202	0.870	0.130	0.123	0.004	0.67	0.20	1	2	2	15	1	20	2	0.67
82	122	204	0.230	0.090	0.032	0.001	2.46	1.93	0	2	0	0	22	20	2	0.00

to filled main shells, i.e., to the magic numbers ($Z, N = 2$, 8, 20, 28, 50, 82, and 126). In principle, below $Z, N = 82$ there are cases where additional "magic" numbers associated with complete filling of of subshells are suggested, e.g., 38, 40, 64. The latter number is related to the filling of the $d_{5/2}$ and $g_{7/2}$ subshells just above $Z, N = 50$. However, we limit ourselves with the generally accepted standard numbers. After these considerations, more general shape/collective effects as well as their interplay with the single-particle ones will be discussed.

1. Single-particle effects

The inspection of Figs. 1, 2 and Table I leads to the identification of nuclei with R values deviating significantly from $R = 1$ as well as with appreciable evolution in R characterizing the respective isotopic chains where data are available. We will separately consider these cases and try to associate them with the population of the Nilsson orbitals evolution for both proton and neutron systems. It should be mentioned that the spherical gaps associated with specific Z, N (at $\epsilon_2 = 0$) are of course modified at larger deformation, i.e., with the increase of ϵ_2 when the spherical subshells split into Nilsson states (cf. Figs. 3, 4, and 5).

In general, the rather complex behavior of R is related largely to proton-neutron interactions different for every (Z, N) pair. The deviations are in most of the cases toward a value $R > 1$ for the transitional and nearly spherical nuclei. Ideally, the quadrupole moment of a spherical nucleus should be zero, with no static deformation, but the quadrupole vibrations as well as other anharmonicities may dynamically induce a small (effective) value of Q. Such values have the tendency to make the ratio R large by the presence of the relatively small $B(E2)_Q$ in the denominator of Eq. (8), indeed. More precisely, the reduced matrix element $\langle I||\tilde{Q}_z||I\rangle$

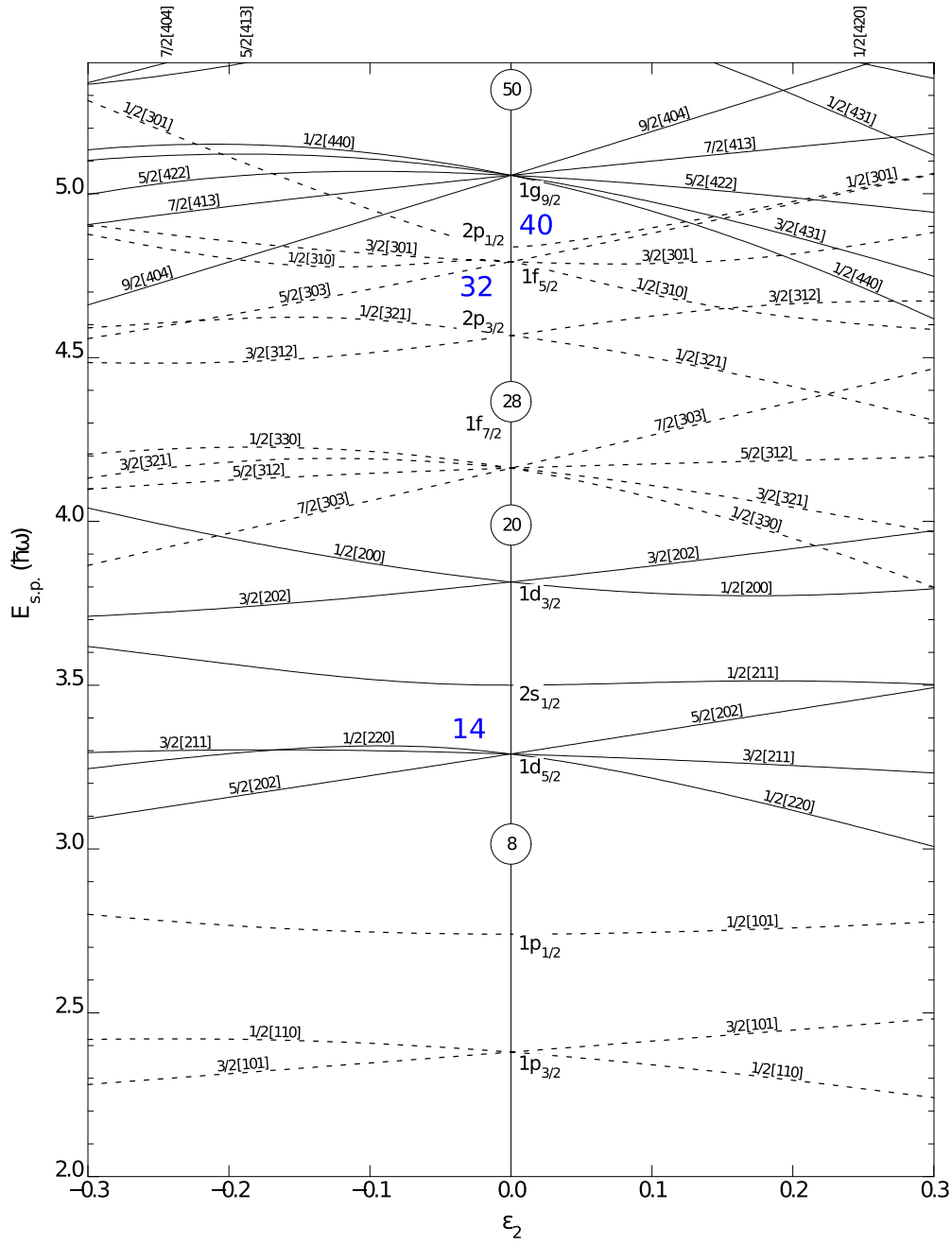

FIG. 3. Nilsson orbitals in the range of 8–50 neutrons in dependence on the quadrupole deformation parameter ϵ_2 ($\epsilon_2 \approx 0.95\,\beta$.).

[Eq. (4)] in the definition of Q is proportional to the sum over the nucleons of the integral of $r^2Y_2^0(\theta,\phi) \propto r^2(3\cos^2(\theta)-1)$ taken between the bra and ket vectors of the state $|I\rangle$ [cf. Eq. (2)]. We remind that the angle θ is measured about the z intrinsic axis and therefore the matrix element considered can be regarded as a measure of the deviation from spherical symmetry. Let us assume that this integral is very small. The reduced matrix element for the transition $I \to I-2$ is proportional to the integral of the same quantity taken between the wave vectors $\langle I-2|$ and $|I\rangle$. Since only the vector $\langle I-2|$ is different, one should expect a somewhat larger value of the integral now, otherwise the transition would not occur. This effect seem to be the reason of the deviations of R toward values larger than 1. Let us consider consecutively such deviations of R with increasing Z in Fig. 2 (when necessary, the observations are combined with the data in Fig. 1 and Table I as well as the filling of the Nilsson orbitals shown in Figs. 3, 4, and 5).:

(i) ^{28}Si: In $^{28}_{14}$Si$_{14}$ both proton and neutron systems fill completely the $1d_{5/2}$ orbitals and these subshell closures lead to a spherical shape, at least at the lowest spins.

(ii) ^{52}Cr: In $^{52}_{24}$Cr$_{28}$ the number of neutrons is magic ($N = 28$) while the protons are in the middle of the $1f_{7/2}$ subshell.

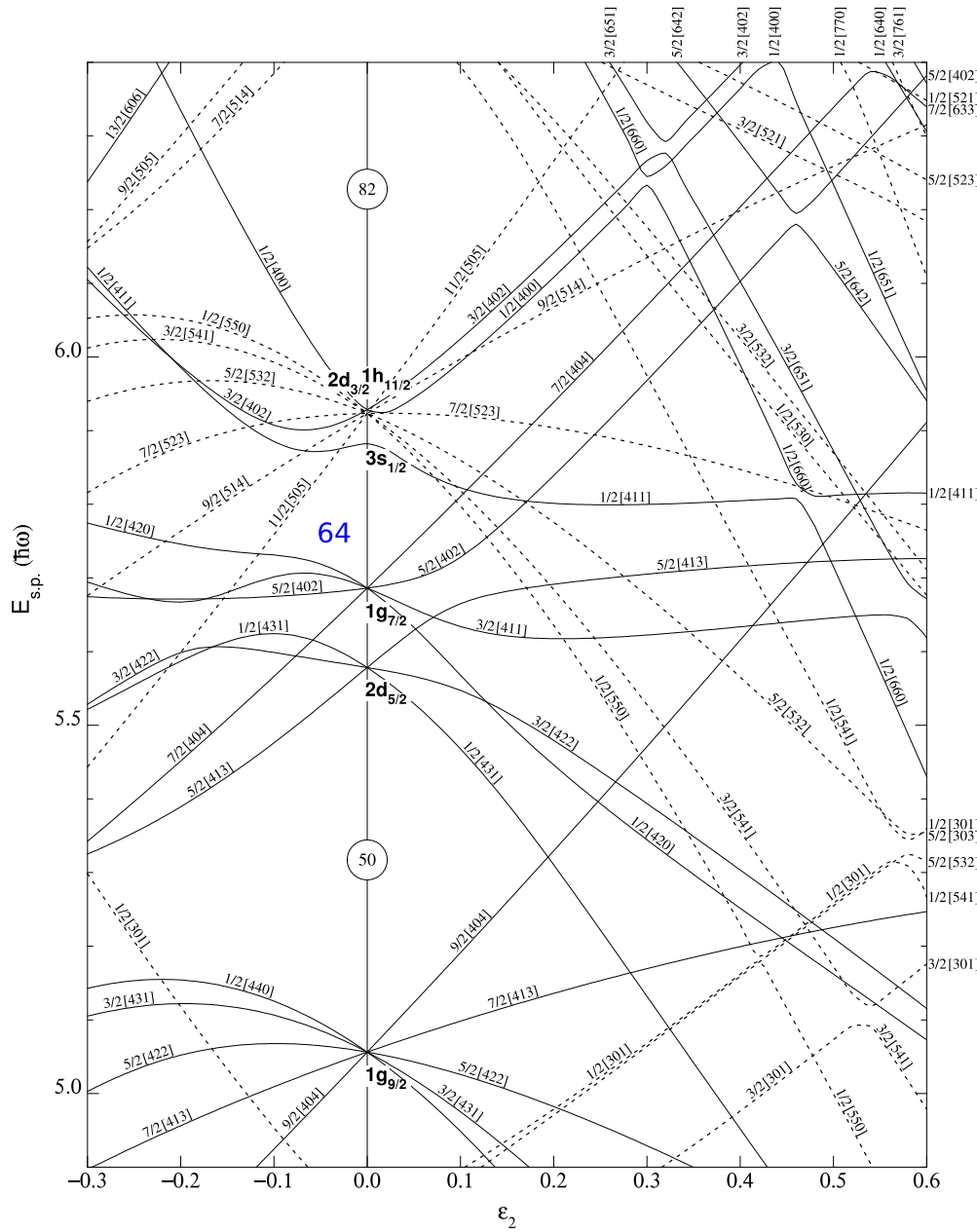

FIG. 4. The same as Fig. 3 but for N from 50 to 82 .

(iii) ^{60}Ni: In $^{60}_{28}$Ni$_{32}$ the number of protons is magic ($N = 28$) while the neutrons fill completely the $2p_{3/2}$ subshell (cf. Fig. 3).

(iv) Ge-Se isotopes: The Ge($Z = 32$) and Se($Z = 34$) isotopic chains presented in Fig. 2 are characterized by the same number of neutrons in the interval $N = 40$–44. However, the behavior of the corresponding R's is quite different. The stabilization (although with fluctuations) toward lower values in Se may be explained by the deformation-driving role of the lowest $1/2[310]$ orbit stemming from the $1f_{5/2}$ shell filled with on the last two protons. Simultaneously, at $N = 40$ all subshells below the $1g_{9/2}$ one are filled, an energy gap appears between $2p_{1/2}$ and $1g_{9/2}$, and the increase of N above 40 leads initially to prolate deformation driving effect which is changed to a preference for oblate deformation when approaching the magic $N = 50$. This picture of somewhat different roles of protons and neutrons with respect to the quadrupole deformation are consistent with the suggested strong, nearly rigid triaxiality [10] close to the ground states in even-even Ge and Se isotopes on the basis of considering the lowest quadrupole invariants of rang 2 and 3 (Q^2 and Q^3, see also below).

(v) Mo-Ru-Pd-Cd isotopes: In the Mo, Ru, Pd, Cd isotopic chains ($Z = 42,44,46,48$, respectively) what was said above for the Ge-Se neutrons can be re-

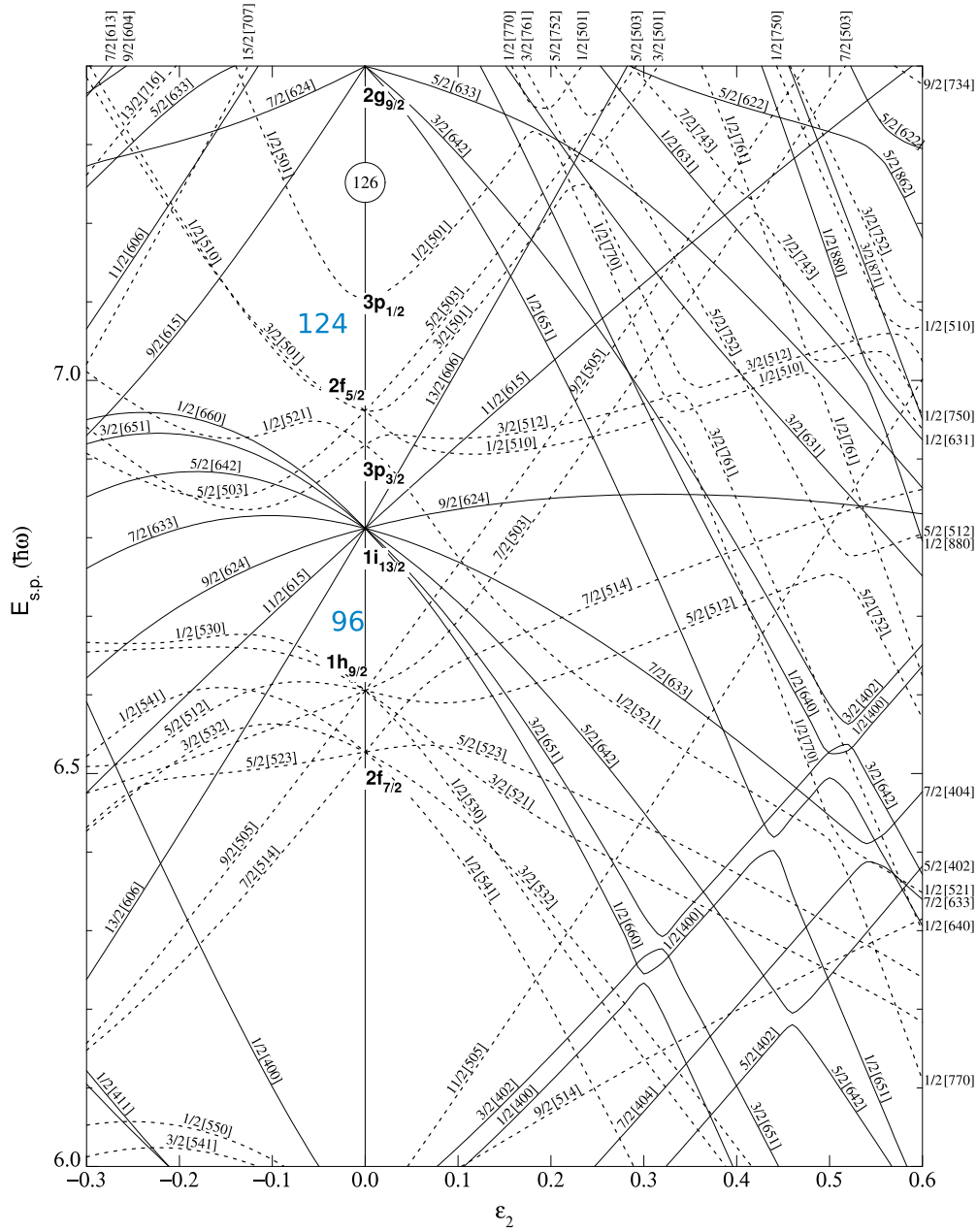

FIG. 5. The same as Fig. 3 but for $N > 82$.

peated, but now with respect to the increase of the proton numbers in the $1g_{9/2}$ subshell toward $Z = 50$. In this group, N changes from 54 in ^{96}Mo to 68 in ^{116}Cd. There is some overlap between the neutron numbers, especially in neighboring isotopes, with $N = 58$ being present in all partial chains considered. This number is positioned about midshell between magic $N = 50$ and the more questionable but quite often suggested magic $N = 64$. It has to be mentioned that the error bars of the data for the Mo and light Ru isotopes are relatively large, but a tendency seems to emerge for low values of R around $N = 58$–60 and even values of $R \approx 1$ are observed in ^{102,104}Ru. However, it would be premature to conclude that the $A = 100$ Ru and Pd nuclei are good rotors, there are attempts to address the properties of these nuclei in terms of features specific for a transition between the U(5) and O(6) limits of the IBA, and in general to find good candidates for the E(5) critical point symmetry [11]. The fact that the inclusion of a g boson in the framework of the IBA leads to a good description of ^{104}Ru [12] points to the role of hexadecapole deformation effects and thus to more complex nuclear shape. The Cd isotopes also display a variety of properties suggesting shape changes (see, e.g., the recent work [13] applying the pseudo-SU(3) model to these isotopes and the Sn ones) while they should be simply vibrator-like nuclei, with some anharmonicities in the collective potential. The high value $R = 5.86$ (2.76) for $^{116}_{50}$Sn$_{66}$

because its magic $Z = 50$ can be hardly surprising. Thus, the Mo-Ru-Pd-Cd region remains a challenge for nuclear theory.

(vi) Te isotopes: In the Te isotopes considered ($Z = 52$), the outermost protons are lying on the deformation driving orbitals stemming from the $2d_{5/2}$-$1g_{7/2}$ subshells. For the interval $A = 122$–130 the occupation of the neutron orbitals undergoes an evolution from slightly above midshell to the $N = 82$ closed shell. This qualitatively explains the evolution of R values from close to the ASR ones to $R = 16.9(14.1)$ in ^{130}Te.

(vii) Ba isotopes: In the Ba ($Z = 56$) isotopes considered ($A = 134$–138), the error bars of the R's are quite large but nevertheless their mean value of about $R = 6$ points to deviations from rigid axial shapes. While the situation with the neutrons seems to be clear (they approach gradually $N = 82$), that with the protons is more complicated. On the one hand, the $2d_{5/2}$ subshell could be fully filled. On the other hand, there are indications that the $1g_{7/2}$ subshell may come down and mix with the $2d_{5/2}$ orbital [14]. Thus, effects driving to prolate deformation may appear, opposite to the effect driven by the last neutrons below and at $N = 82$. In this general framework, experimental evidence for O(6)-like features or γ-soft character of the Ba (and Xe) nuclei was found [15]. Later this picture was somewhat revised (see, e.g., [16]) but still the expectations for high values of R are kept and indicate the deviations from a rigid axial shape.

(viii) Ce-Nd isotopes: In the $^{142}_{58}$Ce$_{84}$ and $^{144-150}$Nd isotopes the high R values at $N = 84$ are obviously related to magicity and with the complications in the proton $2d_{5/2}$-$1g_{7/2}$ subshells mentioned above. The following drop in R in the Nd's toward the ASR value (in some cases even below) has as main reason the gradual filling of the low-Ω neutron orbitals after $N = 82$. These down-sloping orbitals stem from the $2f_{7/2}$, $1h_{9/2}$, and $1i_{13/2}$ in the new shell. The effect is nicely illustrated by the abrupt fall of R to the ASR value in ^{146}Nd down from that in ^{144}Nd.

(ix) Os-Pt-Hg isotopes: These isotopes are positioned at the end of the classical region $150 < A < 190$ of axially deformed nuclei. We remind that we consider $^{184-192}_{76}$Os$_{108-116}$, $^{192-198}_{78}$Pt$_{114-120}$, and $^{198-202}_{80}$Hg$_{118-122}$, As matter of fact, most of the Pt's and all the Hg's among them are out of the classical region. The number of their neutrons gradually gets far from the mid main shell at $N = 104$ and approaches the magic $N = 126$. The behavior of the R values for the platinum isotopes resembles to that of the Se's and Cd's considered earlier—relatively stable R's >1 (with fluctuations within the error bars). This suggest triaxiality effects and indeed, ^{196}Pt was the first nucleus proposed to have an O(6) character [17]. This limiting case of the IBA is associated geometrically with γ-softness and the features of γ-soft rotor [18] as already mentioned. The last four neutrons of ^{196}Pt fill the $3p_{3/2}$ orbits which have a small prolate-driving character with increasing deformation ϵ_2 while the last protons act in the opposite direction. Thus, important prerequisites for γ-softness are available. The latter exist also in the neighboring Os and Hg, however with different balances leading in some cases to oblate shapes (in the Hg isotopes) and shape-coexistence (see below).

2. Considerations within the IBA-2

Let us consider now the data from point of view of one of the most popular and easily accessible to experimentalists for concrete calculations collective models, namely the IBA-2 [9]. Thereby, proton and neutron bosons are distinguished which is not the case for its first version IBA-1. We apply the standard counting of the bosons based on half the distance from the closest for given Z and N magic numbers. In the framework of the IBA-2, the leading role of the proton-neutron quadrupole interaction for the evolution of collectivity is nicely illustrated by presenting the dependence of different observables on the product of proton and neutron boson numbers N_π and N_ν as proposed by Casten [19]. To interpret the results of the application of this $N_\pi N_\nu$ rule shown in Fig. 6, it is convenient to use the columns of Table I starting from the tenth to the up-most right. The simplest observation is that for values of $N_\pi N_\nu > 20$ ($= 4 \times 5$) all R values lie within the error bars on the axial rigid rotor (ASR) line with $R = 1$. These values correspond to the nuclei from the centrum of the deformed region with $Z = 68$ to 76. However, the nuclei above $^{152}_{62}$Sm$_{90}$ but with $Z < 68$ have also R values consistent with the ASR line with much smaller $N_\pi N_\nu$ (and $N_\pi + N_\nu$) values. Of course, the role of ^{152}Sm as pivotal nucleus, namely in the context of the critical point symmetry X(5) [20,21] is well known and is nicely confirmed by our findings. The neighboring two even-even Sm isotopes with smaller number of neutrons ($N = 86,88$) have values of R smaller than 1 which indicates probably shape coexistence phenomena at quite low excitation energy (see also text below, and Table II).

In Fig. 7, the x axis is rescaled compared to that in Fig. 6, namely the quantity $P = N_\pi N_\nu/(N_\pi + N_\nu)$ or the P factor [22] which can be interpreted as a measure of the valence proton-neutron interactions per one boson. The data on the ratios R looks now much more compact and better organized, with the nuclei deviating from the ASR $R = 1$ line grouped mainly in two intervals (approximately 0.5–1.0 and 1.25–1.75). The first interval may be associated with a very close position on the nuclear map to magic number(s) while the second one corresponds to nuclei with more pronounced transitional character (see also Table I).

However, there are other types of mainly quadrupole collectivity expressed by sufficiently large $B(E2)$'s even at small values of Q. In such nuclei, the oscillations of the nuclear surface of quadrupole character, also, vibrations of that type, are more adequate to depict the lowest excited states in even-even nuclei. Some of them preserve the axial symmetry in the intrinsic frame (pure vibrators, U(5) limit nuclei), others do

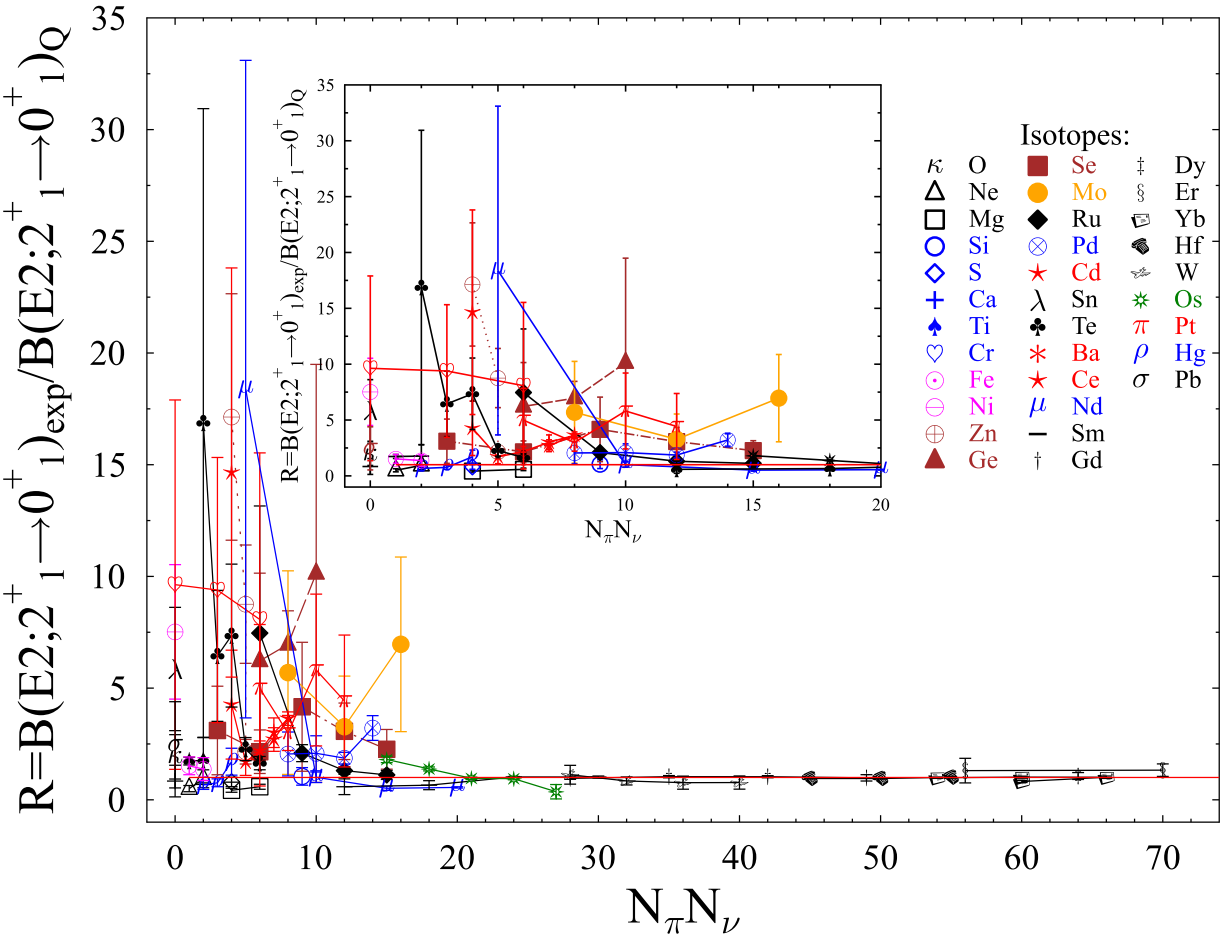

FIG. 6. The same data as in Figs. 1,2 but plotted as function of the product $N_\pi N_\nu$ of IBA bosons associated with half the valence protons (π) and neutrons (ν), respectively. The data points in the isotopic chains, identified by the symbols in the legend, are interconnected by lines. Note that after $N_\pi N_\nu \approx 15 = 5 \times 3 = 3 \times 5$ all ratios R drop down to the ASR line. At smaller $N_\pi N_\nu$'s the situation is more complicated and we tried to make this more clear in the insert $N_\pi N_\nu = 0 \pm 14$. See also text.

TABLE II. Collection of the cases of $R < 1$ values observed among the investigated isotopes. For the meaning of the items in the first nine columns see caption to Table I. The last column contains short comments pointing to the type of shape coexistence discussed in the literature with quotations. See also text.

Z	N	A	Q	ΔQ	$B(E2)$	$dB(E2)$	R	ΔR	Interpretation
10	10	20	−0.230	0.030	0.006	0.001	0.50	0.14	^{20}Ne = $\alpha + {}^{16}$O states interacting with spherical states, [7,24]
12	12	24	−0.290	0.030	0.009	0.000	0.43	0.09	$2\hbar\omega$ contribution to low-lying 0^+ states, [25]
12	14	26	−0.210	0.020	0.006	0.000	0.58	0.11	
16	16	32	−0.160	0.020	0.005	0.000	0.80	0.21	^{32}S = ^{16}O + ^{16}O states interacting with spherical states, [8]
24	26	50	−0.360	0.070	0.021	0.001	0.67	0.26	Spherical-deformed shape coexistence in *pf* shell, [26]
60	86	146	−0.780	0.090	0.150	0.004	1.01	0.23	Striking behavior of the 0_2^+ excitation energy in $^{146-152}$Nd,
60	88	148	−1.460	0.130	0.268	0.006	0.52	0.09	it drops suddenly in ^{150}Nd by $\approx$ 230 keV, then rejumps higher
60	90	150	−2.000	0.050	0.541	0.006	0.56	0.03	X(5) shape-(phase) transition around N=90, [20,21]
62	86	148	−1.000	0.300	0.143	0.007	0.59	0.35	Striking behavior of the 0_2^+ excitation energy in $^{148-154}$Sm, it drops
62	88	150	−1.300	0.200	0.269	0.005	0.65	0.20	suddenly in ^{150}Sm by $\approx$ 680 keV, then remains approximately constant
62	90	152	−1.670	0.020	0.692	0.000	1.02	0.02	in $^{150-152}$Sm, finally rejumps higher (by 400 keV) in ^{154}Sm
62	92	154	−1.870	0.040	0.869	0.001	1.02	0.04	X(5) shape-(phase) transition at N=90, [20,21]
70	106	176	−2.280	0.060	1.038	0.018	0.82	0.05	Coexisting excited 0^+ state with different deformation, [27]
76	108	184	−2.700	1.200	0.643	0.016	0.36	0.32	Experimental problems?
80	120	200	0.960	0.110	0.171	0.006	0.76	0.18	Shape coexistence in the neutron-deficient
80	122	202	0.870	0.130	0.123	0.004	0.67	0.20	lead region: 188 − 200Hg, [28]

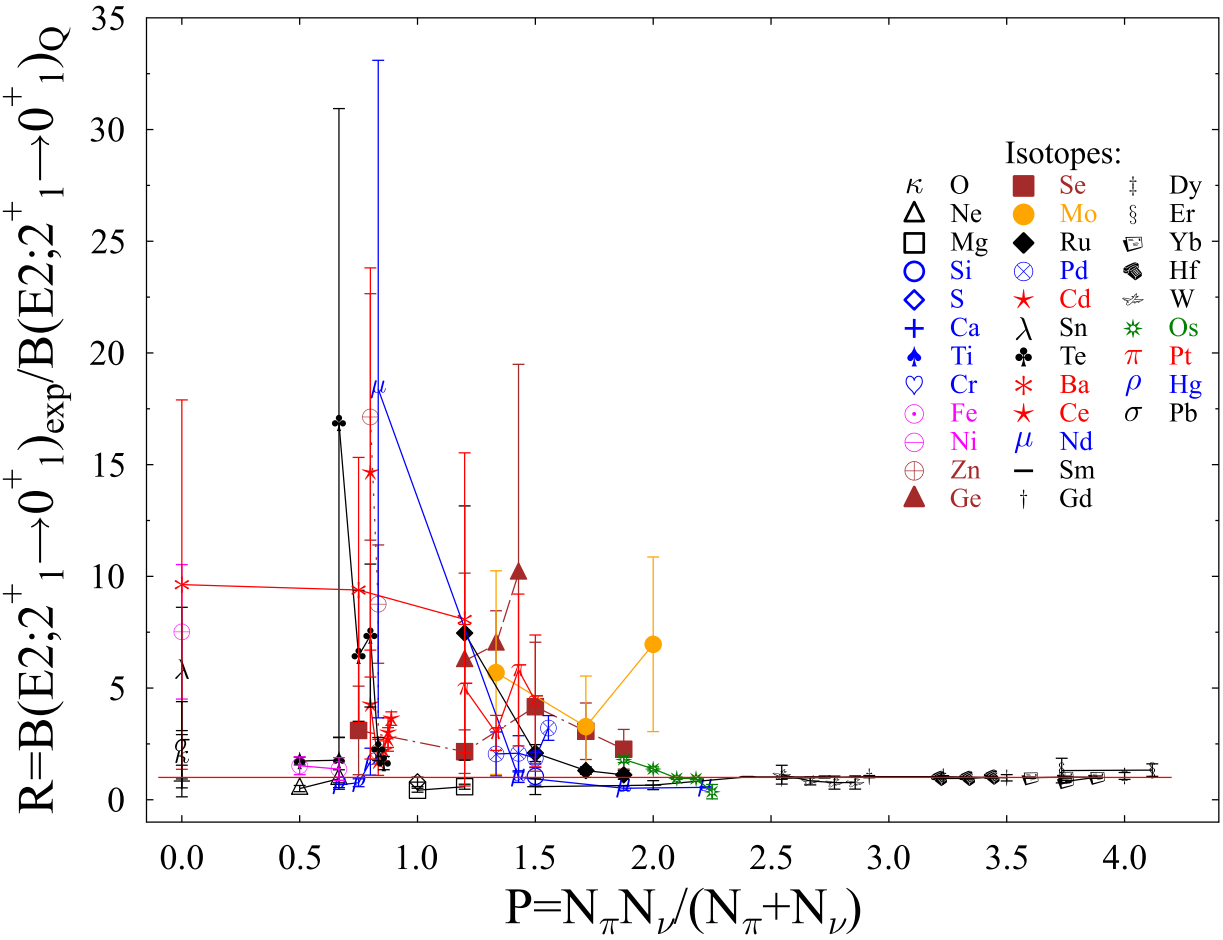

FIG. 7. The same as in Fig. 6 but plotted as function of the normalized product $N_\pi N_\nu/(N_\pi + N_\nu)$ of IBA-2 bosons. See also text.

not [γ-soft rotors, O(6) limit nuclei]. In the context of our study, their R values lie above the ASR line of $R = 1$ and this was discussed above when individual isotopic chains were discussed. The values of the $N_\pi N_\nu$ product in all these cases never surpasses 20 (i.e., when one has four proton and five neutron bosons, or the inverse).

Obviously the ratio R shows a sensitivity to fine effects related to the filling of valence orbitals. Let us turn now our attention again to the cases where the R's have in mean a constant behavior but fluctuations around this mean value are not hard to be seen. The nature of these fluctuations as well as the question if they are related to each other via a common basic physical nature can be posed. The answer to it seems to be rather negative because of different well established interpretations in the literature: the Pt's considered are γ-soft (see, e.g., Refs. [9,17]), the Cd's are anharmonic vibrators (see, e.g., [23]) and the Se's may be rigid triaxial [10].

3. *Cases of $R < 1$: A new signature for shape coexistence?*

In some cases throughout the isotopes considered, values of R distinguishably smaller than 1 are observed. These cases are summarized in Table II. It is not so easy to decide immediately if one is really confronted with a physical effect, nor to find a widely employed nuclear model explaining it. For example the asymmetric rigid rotor model of Davydov and Fillipov [29] predicts R values smaller than 1, but the effect is rather small, varying with γ and being no more than 7%. In most of the cases this effect is within experimental error bars. Here, we will try to address the $R < 1$ values more quantitatively by considering the two lowest quadrupole states 0_1^+, 2_1^+ as a superposition (resulting from mixing) between excitations with different quadrupole deformation, i.e., a case of shape coexistence. An important and very often used assumption in such treatment is that the cross-talk between the two unperturbed excitations via the $E2$ operator is negligible. Let us consider one concrete case, namely when axially deformed states (def) and vibrational (spherical) states (vib) are mixed. Then, the total wave function can be written as

$$|\Psi\rangle = a_{\rm vib}|{\rm vib}\rangle + b_{\rm def}|{\rm def}\rangle. \tag{11}$$

To simplify the discussion, we assume also that the composition of the wave functions of the 2_1^+ and 0_1^+ states is similar with respect to the weights of the unperturbed states $|{\rm vib}\rangle$ and $|{\rm def}\rangle$. Then, the experimental $E2$ reduced matrix element for

the $2_1^+ \to 0_1^+$ transition is given by

$$\langle 0_1^+||E2||2_1^+\rangle_{\rm exp} = b_{\rm def}^2\sqrt{\frac{25}{16\pi}}\langle 2020|00\rangle Q_0 + \left(1-b_{\rm def}^2\right)\langle 0_1^+||E2||2_1^+\rangle_{\rm vib}, \quad (12)$$

where the usual assumption for neglectful contribution of transitions between the deformed and spherical wave-function components is made. Since for vibrational, close to spherical nuclei the spectroscopic quadrupole moment disappears (or is close to zero in a more general case), one has

$$Q(2_1^+)_{\rm exp} = -b_{\rm def}^2\tfrac{2}{7}Q_0. \quad (13)$$

As is well known [4],

$$\langle 0_1^+||E2||2_1^+\rangle_{\rm vib} = \frac{3}{4\pi\sqrt{5}}ZeR^2\beta_2^{\rm vib}, \quad (14)$$

where R is the mean radius of the nuclear sphere and $\beta_2^{\rm vib}$ is the mean amplitude of the shape parameter β for quadrupole vibrations (surface oscillations) conserving the axial shape. It is easy to show that at such conditions our ratio R can be expressed as

$$R = \left|\left(1-b_{\rm def}^2\right)\left(\frac{\beta_2^{\rm vib}}{\beta_2^{\rm def}}\right)^2 + b_{\rm def}^2\right|^2. \quad (15)$$

Since $\frac{\beta_2^{\rm vib}}{\beta_2^{\rm def}}$ is always less than 1, obviously within these mixing assumptions R is close to 1 when the deformed state dominates the wave function ($b_{\rm def}^2 \approx 1$) and can reach even quite small values close to 0, in principle. Therefore, we interpret the experimental values of R which are smaller than 1 with the uncertainties taken into account as a signal for shape coexistence between spherical and deformed states. More precisely, if there is a shape coexistence of the type discussed (between spherical and deformed states), R is for sure less than 1. But we cannot claim that the inverse is always true. For example, one could be confronted with a purely experimental problem of imprecise data.

The data in Table II support such hypothesis, with one exception—the case of ^{184}Os, but there experimental problems might play a role since the relative error of R is close to 100%. It is out of the scope of the present work to investigate in details the nature of the shape coexistence in all cases presented in Table II. A very abundant literature can be found in the references quoted in the table. We use for illustration only few cases from our practice. As shown in [7,8] for ^{20}Ne and ^{32}S, respectively, effects of clusterization (α clusters or larger clusters) may play an important role and lead to shapes different from the classical axially symmetric ellipsoid. More details on clusterization in nuclei in general and in particular for ^{20}Ne can be found, e.g., in [24,30,31]. We mention also that in the Sm and Nd considered, another coexisting shapes come into play around $N = 88$. These are yrast octupole bands (with odd spins) lying quite low in energy [32]. However, because of the negative parity, they do not mix with the quadrupole states. At about $N = 88$, strong octupole effects are expected because of the presence among the valence orbitals of pairs characterized by $\Delta l = 3$ where l is the orbital number in the spherical basis. Such pairs among the neutrons are the $(1i_{13/2}, 2f_{5/2})$ and $(1i_{13/2}, 2f_{7/2})$ ones (see Fig. 5). The parity-alternating yrast bands in ^{144}Ba were thoroughly investigated in Ref. [33] including explicit analytical expressions for $B(E2)$ transitions within the bands. An interesting point in that work is the involvement of clusterized α-particle component in the wave functions. We note that with six neutrons above $N = 82$ and six protons above $Z = 56$ in ^{144}Ba a formation of mixing configuration with three α-particles seems natural. These three α's induce octupole-driving shape effects, indeed.

As already mentioned, and as it also follows from the consideration of Table II, it is not necessary to have always a mixing of spherical and deformed sates to obtain $R < 1$, it is sufficient to have an interaction and mixing between excitations with different quadrupole deformation (i.e., with weak overlap of the wave functions) provided that their cross-talk via the $E2$ operator is negligible.

IV. SUMMARY AND CONCLUSIONS

In conclusion, we have presented a new way to look at the evolution of collectivity on the nuclear map using the ratio $R = B(E2; 2_1^+ \to 0_1^+)_{\rm exp}/B(E2; 2_1^+ \to 0_1^+)_Q$. The systematics of such ratios in even-even nuclei reveal interesting features as signatures for particular collective excitations and sensitivity to shell- and sub-shell closures. Their absolute size appeals for reproduction by nuclear models. A value of $R < 1$ seem to indicate effects of shape-coexistence at low excitation energy in the corresponding nucleus. In our opinion, new measurements of quadrupole moments are needed to enlarge the systematics below $Z < 82$. It is of interest to expand the systematics also for $Z > 82$ after future measurements.

ACKNOWLEDGMENTS

The authors are indebted to I. Ragnarsson, R. Wyss, and V. Werner for very useful discussions.

[1] P. Ring and P. Schuck, *The Nuclear Many-Body Problem* (Springer, Berlin, 1980).
[2] F. A. Majeed, *No-Core Shell Model Calculations for Some Light Nuclei* (Scholar's Press, Riga, Latvia, 2015).
[3] G. C. Bonsignori, M. Bruno, A. Ventura, and D. Vretenar, *Hadrons, Nuclei and Applications* (World Scientific, Singapore, 2001), Vol. 3.
[4] A. Bohr and B. R. Mottelson, *Nuclear Structure* (Benjamin-Cummings, Reading, MA, 1975), Vol. II.
[5] Y. Y. Sharon, N. Benczer-Koller, G. J. Kumbartzki, L. Zamick, and R. F. Casten, Nucl. Phys. A **980**, 131 (2018).
[6] S. J. Q. Robinson, A. Escuderos, L. Zamick, P. von Neumann-Cosel, A. Richter, and R. W. Fearick, Phys. Rev. C **73**, 037306 (2006).

[7] P. Petkov, C. Müller-Gatermann, D. Werner, A. Dewald, A. Blazhev, C. Fransen, J. Jolie, S. Ohkubo, and K. O. Zell, Phys. Rev. C **100**, 024312 (2019).

[8] P. Petkov, C. Müller-Gatermann, A. Dewald, A. Blazhev, C. Fransen, J. Jolie, P. Scholz, K. O. Zell, and A. Zilges, Phys. Rev. C **98**, 019904(E) (2018).

[9] F. Iachello and A. Arima, *The Interacting Boson Model* (Cambridge University Press, Cambridge, 1987).

[10] W. Andrejtscheff and P. Petkov, Phys. Lett. B **329**, 1 (1994)

[11] F. Iachello, Phys. Rev. Lett. **85**, 3580 (2000).

[12] K. Heyde, P. Van Isacker, M. Waroquier, G. Wenes, Y. Gigase, and J. Stachel, Nucl. Phys. A **398**, 235 (1983).

[13] A. P. Zuker, Phys. Rev. C (to be published), arXiv:1905.11479v2.

[14] Jing-ye Zhang, N. Xu, D. B. Fossan, Y. Liang, R. Ma, and E. S. Paul, Phys. Rev. C **39**, 714 (1989).

[15] R. F. Casten and P. von Brentano, Phys. Lett. B **152**, 22 (1985).

[16] L. L. Coquard, N. Pietralla, G. Rainovski, T. Ahn, L. Bettermann, M. P. Carpenter, R. V. F. Janssens, J. Leske, C. J. Lister, O. Möller, W. Rother, V. Werner, and S. Zhu, Phys. Rev. C **82**, 024317 (2010).

[17] J. A. Cizewski, R. F. Casten, G. J. Smith, M. R. Macphail, M. L. Stelts, W. R. Kane, H. G. Börner, and W. F. Davidson, Nucl. Phys. A **323**, 349 (1979).

[18] L. Wilets and M. Jean, Phys. Rev. **102**, 788 (1956)

[19] R. F. Casten, Nucl. Phys. A **443**, 1 (1985)

[20] F. Iachello, Phys. Rev. Lett. **87**, 052502 (2001).

[21] R. F. Casten and N. V. Zamfir, Phys. Rev. Lett. **85**, 3584 (2000).

[22] R. F. Casten, D. S. Brenner, and P. E. Haustein, Phys. Rev. Lett. **58**, 658 (1987).

[23] A. Leviatan, N. Gavrielov, J. E. García-Ramos, and P. Van Isacker, Phys. Rev. C **98**, 031302(R) (2018).

[24] F. Michel, G. Reidemeister, and S. Ohkubo, Phys. Rev. C **37**, 292 (1988).

[25] H. Blok, H. P. Blok, J. F. A. van Hienen, G. van der Steenhoven, C. W. de Jager, H. de Vries, A. Saha, and K. K. Seth, Phys. Lett. B **149**, 441 (1984).

[26] T. Mizusaki, T. Otsuka, M. Honma, and B. A. Brown, Phys. Rev. C **63**, 044306 (2001).

[27] J. E. Garcia-Ramos, V. Hellemans, and K. Heyde, Phys. Rev. C **84**, 014331 (2011).

[28] B. Olaizola *et al.*, Phys. Rev. C **100**, 024301 (2019)

[29] A. S. Davydov and G. Filippov, Nucl. Phys. **8**, 237 (1958)

[30] C. Beck, *Clusters in Nuclei* (Springer, Berlin, 2013), Vol. 3.

[31] F. Michel, S. Ohkubo, and G. Reidemeister, Prog. Theor. Phys. Suppl. No. **132**, 7 (1998).

[32] A. Chakraborty *et al.*, in *Capture Gamma-ray Spectroscopy and Related Topics - Proceedings of the 14th International Symposium*, edited by P. E. Garett and B. Hadinia (World Scientific, Singapore, 2013), p. 556.

[33] T. M. Shneideman, R. V. Jolos, R. Krücken, A. Aprahamian, D. Cline, J. R. Cooper, M. Cromaz, R. M. Clark, C. Hutter, A. O. Macchiavelli, W. Scheid, M. A. Stoyer, and C. Y. Wu, Eur. Phys. J. A **25**, 387 (2005).